The Open University

Open Research Online

The Open University's repository of research publications
and other research outputs

One of the earliest refractory inclusions and its implications for solar system history

Journal Item

oro.open.ac.uk

Journal Pre-proofs

One of the earliest refractory inclusions and its implications for solar system history

Jean-David Bodénan, Natalie A. Starkey, Sara S. Russell, Ian P. Wright, Ian A. Franchi

Please cite this article as: Bodénan, J-D., Starkey, N.A., Russell, S.S., Wright, I.P., Franchi, I.A., One of the earliest refractory inclusions and its implications for solar system history, *Geochimica et Cosmochimica Acta* (2020), doi: https://doi.org/10.1016/j.gca.2020.06.034

One of the earliest refractory inclusions and its implications for solar system history

Jean-David Bodénan[1*], Natalie A. Starkey[2], Sara S. Russell[3], Ian P. Wright[2], Ian A. Franchi[2].

[1]ETH Zürich, Institute für Geochemie und Petrologie, Clausiusstrasse 25, 8092, Zürich, Switzerland.

[2]Planetary and Space Sciences, School of Physical Sciences, The Open University, Milton Keynes, MK7 6AA, United Kingdom.

[3]Department of Earth Sciences, Natural History Museum, Cromwell Road, London, SW7 5BD, United Kingdom.

*Correspondence should be addressed to J.-D. Bodénan (jean-david.bodenan@erdw.ethz.ch).

Postal address: ETH Zürich, Institute für Geochemie und Petrologie, NW D 85, Clausiusstrasse 25, 8092, Zürich, Switzerland.

Phone number: (+41) 446 327 713

Abstract: A ~175 μm refractory inclusion, A-COR-01 from one of the least altered carbonaceous chondrites, ALHA 77307 (CO3.0), has been found to bear unique characteristics that indicate that it is one of the first solids to have formed at the very birth of the solar system while isotopic reservoirs were still evolving rapidly. Its core is composed mainly of hibonite and corundum, the two phases predicted to condense first from a gas of solar composition, and like many common types of Calcium-, Aluminium-rich Inclusions (CAIs) is surrounded by a rim of diopside.

Core minerals in A-COR-01 are very ^{16}O-rich ($\Delta^{17}O_{Core}$ = -32.5 ± 3.3 (2SD) ‰) while those in the rim display an O isotopic composition ($\Delta^{17}O_{Rim}$ = -24.8 ± 0.5 (2SD) ‰) indistinguishable from that found in the vast majority of the least altered CAIs. These observations indicate that this CAI formed in a very ^{16}O-rich reservoir and either recorded the subsequent evolution of this reservoir or the transit to another reservoir. The origin of A-COR-01 in a primitive reservoir is consistent with the very low content of excess of radiogenic ^{26}Mg in its core minerals corresponding to the inferred initial $^{26}Al/^{27}Al$ ratio (($^{26}Al/^{27}Al)_0$ = (1.67 ± 0.31) × 10^{-7}), supporting a very early formation before injection and/or homogenisation of ^{26}Al in the protoplanetary disk. Possible reservoir evolution and short-lived radionuclide (SLRs) injection scenarios are discussed and it is suggested that the observed isotope composition resulted from mixing of a previously un-observed early reservoir with the rest of the disk.

Keywords: Refractory inclusions, O-isotopes, Mg-isotopes, mineralogy, Early Solar System.

1. Introduction

It is widely accepted that the solar system formed by the collapse of a dense molecular cloud core (e.g., Boss and Goswami, 2006 and references therein) that was part of an active star formation region. This undoubtedly led to chemical and isotopic variations at multiple geometric and temporal scales. Some materials in the most primitive meteorites were created as these reservoirs were forming and evolving and therefore offer a window into the conditions and processes dominating the early evolution of the protoplanetary disk at the time soon after its formation (< 1 Myr, Mishra and Chaussidon, 2014). Calcium-Aluminium-rich Inclusions (CAIs) formed in the very earliest times of solar system history, and chondrules mainly formed up to a few million years later; although the formation age of some of them overlap with that of CAIs (e.g., Connelly et al., 2012; Bollard et al., 2017; Marrocchi et al., 2019)). The stable isotope compositions of such early solar system products provide a testament to their history, chronology and formation environment.

The measurement of material recovered from the Genesis mission allowed the first direct measurement of the solar oxygen-isotope composition ($\Delta^{17}O$ = -28.4 ± 3.6 ‰; McKeegan et al. (2011), where $\Delta^{17}O$ is the departure from the Terrestrial Fractionation Line (TFL) as calculated by the formula $\Delta^{17}O = \delta^{17}O - (0.52 \times \delta^{18}O)$. This value is lighter than most CAIs and provides an important step in understanding the initial O-isotope composition of the protoplanetary disk and the processes that modified the reservoirs from which the rocky bodies we observe today formed.

The CAI population is made up of remarkable objects displaying a range of isotope compositions (notably O, Mg, Ca, and Ti) and different mineralogies and petrologies, resulting from varied histories in the early solar system. Corundum- and/or hibonite-bearing inclusions are among the most refractory of these inclusions (Bar-Matthews et al., 1982; Simon et al.,

2002; Makide et al., 2013), with corundum being among the very first phases predicted to form in the hot inner regions of the early solar system, followed by hibonite (Yoneda and Grossman, 1995; Petaev and Wood, 1998; Ebel and Grossman, 2000). They have primarily been studied in CM chondrites, such as Murchison and Murray (Bar-Matthews et al., 1982; Fahey et al., 1987a; Fahey et al., 1987b; Simon et al., 2002; Makide et al., 2013) and, while the corundum-bearing CAIs are very rare, the hibonite-bearing inclusions are relatively common. Depending on the mineralogy and textures, the hibonite-bearing inclusions have been classified into several groups, including platy hibonite crystals (PLACs), spinel-hibonite-perovskite inclusions (SHIBs) and blue aggregates (BAGs) (Ireland, 1988). More recently, a new group of objects, labelled as PLAC-like CAIs, has been defined, describing CAIs related to PLACs (Kööp et al., 2016a). These groups have been reported to display different signatures in isotopic systems such as Ti, Mg, and Ca (e.g., Ireland, 1988; Kööp et al., 2016a, 2016b, Liu et al., 2012, 2009). The O-isotope compositions in these inclusions range from nearly 'solar' ^{16}O-rich to ^{16}O-poor, chondritic, values.

Given the short lifetime of some short-lived radionuclides (SLRs) such as ^{26}Al ($\sim$ 0.7 Myr), it has been suggested that SLRs were injected into the early solar system from an external source (Simon et al., 2002; Kita et al., 2013; Makide et al., 2013) with a brief and finite duration (Podosek, 2005). This external source is still a matter of debate. One of the favoured hypotheses for the origin of SLRs are Type II supernovae (e.g., Foster and Boss, 1997; Ouellette et al., 2009). Injection could have occurred when a supernova triggers the collapse of the solar molecular cloud ("trigger model", Cameron and Truran, 1977), or shortly after solar system formation ("aerogel" model). In both cases, homogenisation of SLRs could be achieved relatively fast ($\leq 10^5$ years, Ouellette et al., 2009).

Another possible source being discussed is an AGB (Asymptotic Giant Branch) or a Super-AGB star (mass range of 7-11 $M_\odot$, e.g., Lugaro et al., 2012; Wasserburg et al., 1994). The

latter could produce the abundances of ^{26}Al, ^{41}Ca, and ^{60}Fe observed in meteorite records, within the uncertainty of proposed models. Wolf-Rayet stars have also been suggested as a possible origin for the SLR contaminating the early solar system (e.g., Arnould et al., 2006), and has recently gained prominence as a possible origin for SLRs (e.g., Kaur and Sahijpal, 2019).

Considering the Al-Mg system alone is not sufficient to distinguish between these hypotheses. Coupling Mg isotope analyses with other isotopes, such as O-isotopes, allows for more constraints and could help to assess which model is most plausible. If the material that carried ^{26}Al into the solar system had different O isotopic composition, it could impact the O isotopic composition of the reservoirs in which CAIs formed and could explain part of their evolution.

Among previously studied corundum and hibonite-bearing inclusions, two populations can be defined based on their Mg-isotope composition. Inclusions in the first group display the canonical initial ^{26}Al/^{27}Al ratio ((^{26}Al/^{27}Al)$_0$) of ~5 × 10^{-5} (MacPherson et al., 1995) while others display no resolvable ^{26}Mg excess from the decay of ^{26}Al (^{26}Mg*) ((^{26}Al/^{27}Al)$_0$ < 5 × 10^{-6}). These observations have been interpreted as a record of ^{26}Al/^{27}Al heterogeneity in the early solar system either in time or in space (Kita et al., 2013; Makide et al., 2013; Kööp et al., 2016a; Kööp et al., 2016b).

The present study focuses on a corundum-hibonite-bearing inclusion surrounded by a diopside rim from the CO meteorite Allan Hills A-77307 (ALHA-77307). ALHA-77307 is one of the most primitive samples in the CO3 group and has been classified as a CO3.0 (Scott and Jones, 1990) on the basis of type I chondrule petrography, and the composition of olivine in Amoeboid Olivine Aggregates (AOA, Chizmadia et al., 2002). Cr_2O_3 and S contents also suggest the same classification (Grossman and Brearley, 2005). Although, this classification has been debated in comparison to more pristine CO chondrites Dominion Range (DOM) 08004 and DOM 08006. A number of petrographic indicators of metamorphism, including the structural

ordering of organic matter (Bonal et al., 2007), also indicate that this meteorite is one of the least affected by thermal metamorphism in the CO3 group. The lack of phyllosilicates in the matrix of ALHA 77307 indicates that this meteorite has experienced very little, if any, aqueous alteration. Thus, it is an ideal sample for studying refractory inclusions without the complications linked to secondary processes that took place on the CO parent body.

O and Mg-isotopes were analysed in-situ in different phases of this inclusion to better constrain the conditions and evolution of early reservoirs in the protoplanetary disk.

2. Materials and methods

2.1. Scanning Electron Microscopy

A FEI Quanta 200 3D scanning electron microscope (SEM) at The Open University (Milton Keynes, UK) was used to acquire backscattered and secondary electron images. The SEM is equipped with an Oxford Instrument X-Max X-ray detector that was used to obtain elemental energy-dispersive X-ray maps of the samples. A voltage of 20 kV was used with a probe current of 0.60 nA. Combined Mg, Ca and Al Kα elemental maps were used to identify CAIs and their mineral phases.

2.2. Electron microprobe analysis

Major element compositions were measured using a Cameca SX 100 electron microprobe at the Open University (Milton Keynes, UK). A 2 μm beam with an acceleration voltage of 20 kV and an intensity of 20 nA was used. TAP (Thallium Acid Phthalate), LTAP (large TAP), LLIF (Large Lithium Fluoride), PET (Pentaerythritol) and LPET (Large PET) crystals were used to acquire major element composition of analysed phases. Matrix corrections were applied using the PAP model (Pouchou and Pichoir, 1987).

2.3. NanoSIMS isotope measurements

The Cameca NanoSIMS 50L at the Open University (Milton Keynes, UK) was used to measure the O and Mg isotopic ratios in the studied CAI. The NanoSIMS uses the dynamic SIMS (Secondary Ion Mass Spectrometry) method. Its unique geometry allows for small probe sizes that are essential for the analysis of small crystals, notably corundum and the diopside rim (< 10 μm in width).

O-isotopes – A Cs^+ ion beam was used to analyse O-isotopes. A 3×3 μm spot with a pre-sputter area of 5×5 μm was selected. With a probe current of 50pA, sample areas were pre-sputtered for 3 minutes and analyses lasted 5 minutes.

Secondary ions of the three oxygen-isotopes, $^{16}O^-$, $^{17}O^-$ and $^{18}O^-$, were measured as well as $^{24}Mg^{16}O$ and $^{40}Ca^{16}O$ to confirm which phase was analysed. $^{16}O^-$ was measured using a Faraday cup because of the high count rate for this isotope ($>10^7$ counts per second) but all other species were measured on electron multipliers (EM). The instrument was set to give a mass resolving power >10000 (Cameca NanoSIMS definition) on the EM detector used to measure $^{17}O^-$, sufficient to resolve the $^{16}OH^-$ peak from that of $^{17}O^-$ (contribution of $^{16}OH^-$ was typically around 25 ppm). All analyses were normalised to a mineral standard matched for elemental composition to provide appropriate corrections for matrix effects and instrumental mass fractionation (IMF). Oxygen-isotopes results are reported as $\delta^{17}O$ and $\delta^{18}O$, representing per mil deviations from SMOW (Table 1). Typical count rates are 1.1×10^7 for $^{16}O^-$.

Charge compensation during the analyses was achieved with an electron gun. Errors are reported as 2SD and include the measurement internal uncertainty and the external reproducibility from standards analysed before and after each group of measurements.

At least five spots were analysed using NanoSIMS in the standards before and after the analysis of the corresponding mineral in a sample to correct for matrix effect and IMF. The terrestrial

standard analyses fall on the TFL and cluster tightly for each mineral indicating a reproducibility of typically of 2.5‰ for $\delta^{17}O$ and 1.5‰ for $\delta^{18}O$ (2SD errors).

Burma spinel, hibonite, diopside, and a sapphire glass were used as the standards for spinel, hibonite, diopside, and corundum, respectively. The composition of each of these standards was measured by EDX with a FEI Quanta 200 3D and their oxygen isotopic ratios were measured on the oxygen laser-assisted fluorination system at the Open University following the method described in Miller et al. (1999). The results are summarised in Supplementary Table A1.

Mg-isotopes – Mg-isotopes were analysed using an O^- ion beam from the Duo Plasmatron. A probe current of approximately 20 pA was used for all Mg isotopic analyses with an analysis time of ~23 minutes. A 3×3 μm spot with a pre-sputter area of 5×5 μm was selected.

For the high $^{27}Al/^{24}Mg$ ratio phases such as corundum ($^{27}Al/^{24}Mg \geq 810$) and hibonite ($^{27}Al/^{24}Mg \geq 20$), $^{24}Mg^+$, $^{25}Mg^+$, and $^{26}Mg^+$, and $^{44}Ca^+$ were measured on EMs and $^{27}Al^+$ was measured using a FC to accommodate for the high counts. As for O isotopic analyses, the MRP was set to over 10000. $^{27}Al/^{24}Mg$ ratios were corrected using sensitivity factors defined for each measurement session, using Al/Mg measured by EPMA on the standard.

The same single crystals of Madagascar hibonite that were used for O-isotopes were used to standardise both hibonite and corundum. No Mg could be measured in the artificial sapphire glass used for O-isotopes. The Mg isotopic composition of the standards is assumed to be identical to the terrestrial value measured by Catanzaro et al. (1966). Typical count rates for hibonite were 1.9×10^4 for ^{24}Mg, 2.4×10^3 for ^{25}Mg, 2.6×10^3 for ^{26}Mg, and 8.5×10^5 for ^{27}Al, resulting in typical total counts of 2.1×10^7 for ^{24}Mg, 2.6×10^6 for ^{25}Mg, 2.8×10^6 for ^{26}Mg, and 9.2×10^8 for ^{27}Al. In corundum, typical count rates were 3.6×10^2 for ^{24}Mg, 4.5×10^1 for

^{25}Mg, 5.0×10^1 for ^{26}Mg, and 1.4×10^6 for ^{27}Al, resulting in total counts of 3.9×10^5 for ^{24}Mg, 4.8×10^4 for ^{25}Mg, 5.4×10^4 for ^{26}Mg, and 1.5×10^9 for ^{27}Al, typically.

All positions of NanoSIMS spots were checked on high-resolution (0.1 μm/px) backscattered electron (BSE) images (Fig. 1). Points that sampled a mix of phases as well as points positioned in cracks were rejected. Further analytical considerations can be found in Supplementary Material A1.

3. Results

3.1. Mineralogy and petrography

A-COR-01 (Figs. 1-2) is a 175×140 μm-sized sub-rounded CAI, composed of hibonite, corundum, spinel, and diopside. Hibonite is the dominant mineral in the core of the CAI and forms a densely packed mass of lath-shaped crystals. It contains $0.7 - 5.3$ wt.% TiO_2 and 0.3-4.0 wt.% MgO (Table 1). Corundum occurs within hibonite and consists of anhedral grains 5 - 10 μm in size. Its major element composition barely deviates from the ideal Al_2O_3 composition (99.3 - 99.0 wt.% Al_2O_3).

The hibonite-corundum core is surrounded by spinel with a composition very close to the magnesian end member ($0.25 – 0.28$ wt.% FeO, $0.27 – 0.28$ wt.% Cr_2O_3).

A rim of diopside, typically 5 μm wide, but reaching up to 10 μm in places, surrounds A-COR-01. It contains $2.0 – 3.7$ wt.% Al_2O_3 and $1.4 – 2.2$ wt.% TiO_2. In most places, the rim is not in direct contact with the CAI itself in this thin section because a crack 1-4 μm wide separates the diopside layer from the spinel (Figs. 1-2, see Supplementary Figure A2 for zoomed-in view). While it is possible that a missing mineral phase was originally filling this void, which was later removed by secondary processes, this is considered unlikely as such a process should also have affected the other phases to some extent. It is more likely that there was a mechanical

separation of the rim from the CAI during an energetic event, possibly an impact during or after accretion. The matching shape of the outer edge of the spinel and the internal edge of the diopside layer seem to favour this hypothesis.

3.2. Oxygen-isotopes

Oxygen-isotope measurements acquired in A-COR-01 (Table 2) show a bimodal distribution (Fig. 3), with the phases in the core, i.e. corundum, hibonite and spinel, being more enriched in ^{16}O than the rim diopside. The core minerals display a rather limited range of oxygen isotopic compositions, barely exceeding the uncertainty of the measurements, with an average $\Delta^{17}O$ of = -31.2 ± 3.0 (2SD) ‰ for corundum, average $\Delta^{17}O$ = -33.5 ± 2.3 (2SD) ‰ for hibonite, and an average of $\Delta^{17}O$ = -31.2 ± 3.4 (2SD) ‰ for the spinel. The overall mean composition for the core phases is $\Delta^{17}O_{Core}$ = -32.5 ± 3.3 (2SD) ‰. In contrast, the mean composition of the rim diopside $\Delta^{17}O_{Rim}$ = -24.8 ± 0.5 (2SD) ‰.

The rim diopside have average $\delta^{17}O$ and $\delta^{18}O$ of -47.2 ± 0.3 (2SD) ‰ and -43.0 ± 1.5 (2SD) ‰, respectively (Fig. 3), a composition that falls slightly to the right of the Carbonaceous Chondrites Anhydrous Minerals line (CCAM, Clayton et al., 1977), as defined by O isotope compositions of anhydrous minerals from CCs, the Young and Russell line (Y&R), representative of unaltered CAI minerals (Young and Russell, 1998), and the Primitive Chondrule Mineral (PCM, Ushikubo et al., 2012) line, defined from the O-isotope composition of chondrule silicates from Acfer 094.Fine-grained CAIs (Ushikubo et al., 2017) and chondrule relic grains akin to AOAs also fall on this line (Marrocchi et al., 2018; Marrocchi et al., 2019). In contrast, the core phases have O-isotope compositions that plot between 4 and 10 ‰ in $\delta^{18}O$ to the right of the CCAM line (Figure 3). That similar signatures are recorded for three different phases, calibrated against two different standards eliminates the possibility that the offset from the CCAM line is a result of calibration or un-accounted matrix effects.

No clear trends have been observed between O-isotopes and major element compositions.

3.3. Magnesium-isotopes

All Mg isotope results are presented in Table 3 and in Figures 4a, and 4b. Historically, the notations for Mg isotope ratios have been different from the ones used for other light stable isotopes, and use Δ notation for isotope ratios. For consistency, the same notation used for O-isotopes is used throughout this study for Mg-isotopes, where δ notations reflect isotope ratios.

In a Mg three-isotope diagram (Fig. A1.3), hibonite analyses plot within error, or very close to, the kinetic and equilibrium fractionation lines. Hibonite results have a limited range of $\delta^{25}Mg$ (-17.3 ± 1.9 to -14.4 ± 2.0 ‰) and a larger spread of $\delta^{26}Mg$ (-36.9 ± 2.2 to -22.9 ± 2.7 ‰). The very low Mg content of the corundum grains (≤ 0.1 wt.% MgO) results in large uncertainties but both samples are indistinguishable from the hibonite compositions within the uncertainties possible, with $\delta^{25}Mg$ = -18.3 ± 10.2 (2SD) ‰; $\delta^{26}Mg$ = -22.3 ± 9.7 (2SD) ‰ and $\delta^{25}Mg$ = -41.3 ± 34.7 (2SD) ‰; $\delta^{26}Mg$ = -3.7 ± 32.6 (2SD) ‰ (Fig. A1.3).

The $\delta^{26}Mg$ of the hibonite and corundum are very low relative to typical solar system materials. This is most likely linked to matrix effects linked to the difference of composition between sample and standard hibonite. While it prevents using these ratios to discuss potential solar system reservoirs, it shouldn't affect inferred ages from Al-Mg systematics (e.g., Kööp et al., 2017).

Hibonite results for $\delta^{26}Mg^*$ plot between $\delta^{26}Mg^*$ = 7.8 ± 3.3 (2SD) ‰ and -4.7 ± 3.2 (2SD) ‰. Values for the two measured points in corundum are 75.5 ± 47.6 (2SD) ‰ and 13.5 ± 14.0 (2SD) ‰. The fractionation law used to calculate these values is the so-called exponential law β = 0.511 (Russell et al., 1978; Kita et al., 2013; Davis et al., 2015).

4. Discussion

4.1. Formation history of A-COR-01

Corundum grains are found within the hibonite suggesting that corundum formed first by condensation and then reacted with the surrounding nebular gas to form hibonite (Yoneda and Grossman, 1995; Simon et al., 2002; Needham et al., 2017), as expected by predicted condensation and reaction sequences (Yoneda and Grossman, 1995; Petaev and Wood, 1998).

On BSE images (Figs. 1, 5), hibonite crystals display lighter grey tones indicative of compositional zoning at their border. The element most likely to explain this zoning is Ti as it is quite variable (0.7 – 5.3 wt.%). Such disequilibrium in the Ti distribution strongly indicates that there has been little or no re-heating of this inclusion since it has formed, because if hibonite in A77307-COR-01 had been re-equilibrated after its original formation, Ti would most likely have been re-distributed in the crystals and this zoning would have been erased.

From condensation calculations (Yoneda and Grossman, 1995), spinel should condense after melilite but the latter is missing. Condensation of spinel before melilite can be explained by models of condensation with partial isolation (CWPI) (Petaev and Wood, 1998) if the nebular gas was already depleted in Al by the prior condensation of corundum and calcium aluminates. Another explanation would be that spinel grows on hibonite to accommodate Al excess resulting from incomplete condensation of corundum during disequilibrium condensation from a supercooled nebular gas (Han et al., 2015).

The textures of hibonite and corundum in A-COR-01 are similar to those of PLAC hibonite grains (e.g., Ireland, 1988; Liu et al., 2009). However, A-COR-01 is not a single platy crystal, leading to the classification of this inclusion as a PLAC-like CAI. It is, however, possible that PLAC hibonite grains could have originated from the breakdown of similar inclusions (e.g., Kööp et al., 2016a).

4.2. Extreme ^{16}O-rich composition of core minerals

Core minerals, corundum, hibonite and spinel in A-COR-01 display large enrichments in ^{16}O ($\Delta^{17}O_{Core}$ = -32.5 ± 3.3 (2SD) ‰) relative to most compositions reported for CAIs, even in the phases displaying the most undisturbed ^{16}O-rich signatures such as spinel where typically $\Delta^{17}O$ ~ -24 ‰ (e.g., Itoh et al., 2004).

Corundum in A-COR-01 displays O isotope compositions (-33.3 ± 2.6 ≤ $\Delta^{17}O$ ≤ -30.0 ± 2.6 ‰) distinct to those found in even the most ^{16}O-rich corundum in other CAIs (-26.4 ± 2.5 ‰ ≤ $\Delta^{17}O$ ≤ -6.2 ± 21.0 ‰), although they overlap with the composition of some isolated solar corundum grains (-31.2 ± 8.3 ‰ ≤ $\Delta^{17}O$ ≤ -5.3 ± 8.0 ‰) (Simon et al., 2002; Makide et al., 2009; Makide et al., 2013; Needham et al., 2017). The ^{16}O-rich signature in A-COR-01 is similar to the solar value measured from solar winds sampled by the *Genesis* mission ($\Delta^{17}O$ = -28.4 ± 3.6 ‰; McKeegan et al., 2011). The similarity between the ^{16}O-rich composition of A-COR-01 corundum and the Sun supports the interpretation that this mineral formed by condensation of a gas of solar composition. The high temperatures required to form CAI minerals (~1200-1770 K at P_{tot} = 10^{-3} bar, Petaev and Wood, 2005), and especially corundum (~1770 – 1740 K), indicate that such condensation likely occurred close to the protosun.

Previous analyses of O-isotopes in hibonite from SHIBs and PLACs show $\Delta^{17}O$ values ranging from -28.4 ± 1.3 ‰ to -9.8 ± 7.0 ‰ (Liu et al., 2009; Makide et al., 2013; Kööp et al., 2016a; Kööp et al., 2016b; Needham et al., 2017). Results of O isotopic analyses in hibonite in A-COR-01 display a more ^{16}O-rich composition, with an average $\Delta^{17}O$ value of -33.5 ± 3.7 ‰. The group of hibonite displaying the closest isotopic compositions to the ones observed in A-COR-01 are the PLAC and PLAC-like hibonites (Liu et al., 2009; Kööp et al., 2016a). In addition to similar textures, this supports the hypothesis that this inclusion formed by the same processes that have been suggested for PLACs, that of evaporation and condensation close to the protosun, and that PLACs could be fragments of such inclusions.

The highly ^{16}O-enriched compositions for hibonite and spinel could be explained by very early formation of the hibonite and spinel in the sample, probably shortly after the A-COR-01 corundum, and may have formed prior to the formation of the most ^{16}O-rich solar corundum grains previously measured (Simon et al., 2002; Makide et al., 2013).

Equilibration between primordial dust and gas with different O isotope compositions has also been suggested (Kobayashi et al., 2003; Krot et al., 2010) to explain the different O isotope signatures in early solar system objects. Galactic chemical evolution models (Clayton, 1988; Meyer, 2013) predict that nebular gas could have a more ^{16}O-rich composition than co-existing dust (Krot et al., 2010). The isotopic composition difference is a function of the relative average age of the gas and dust resulting from the galactic isotope evolution recorded in these two components Another source of heterogeneity could be the processing of primordial dust and water that could create change sin $\Delta^{17}O$ (Alexander et al., 2017). Such an early heterogeneity has also been suggested to explain $\Delta^{17}O$ variations observed in PLAC-like CAIs by Kööp et al. (2016a) which could also be linked to the O isotopic composition of A-COR-01, especially if it is the type of objects from which PLACs originated. Such an environment could be found close to the Sun, which would be where the high temperatures at which corundum and hibonite condense. We suggest that the primordial, unequilibrated gas could explain the shift to the right of the reference lines in inclusions that could have formed in this reservoir.

The O-isotope compositions of hibonite, spinel, and corundum in A-COR-01 plot to the right of an extension of the CCAM or Y&R lines. Similar compositions have also been observed in PLAC hibonites (Kööp et al., 2016a), although the origin of this O-isotope anomalous compositions is still unclear. It has been suggested that they could result from mass-dependent processes, like melt evaporation, or that this signature could be inherited from an original solar (and dust) composition (Kööp et al., 2016a) that was not on the CCAM or Y&R lines.

This is the first time such a ^{16}O-rich inclusion is found outside the CH/CB chondrites (Kobayashi et al., 2003; Krot et al., 2008; Gounelle et al., 2009), suggesting that such inclusions could be more widespread than previously considered.

4.3. Oxygen-isotope and major element composition of the diopside rim.

The O isotopic composition of the diopside rim surrounding A-COR-01 is different from that recorded in the corundum, hibonite and spinel. While the average value for these core minerals is $\Delta^{17}O_{Core}$ = -32.5 ± 3.3 (2SD) ‰, the composition of diopside in the rim is $\Delta^{17}O_{Rim}$ = -24.8 ± 0.5 (2SD) ‰. This difference requires a change in the composition of the O isotope reservoir in the surrounding environment between the formation of the inclusion core and that of its rim. Two hypotheses can be considered. Either the CAI remained in a limited region of the solar system throughout its entire formation, and this reservoir saw its O isotope composition change with time (hypothesis 1), or, the CAI formed in an more ^{16}O-rich reservoir and transited to a less ^{16}O-rich reservoir between the formation of the core and rim (hypothesis 2).

There is an extensive data set reported in the literature showing that primary phases such as spinel in the least altered CAIs has $\Delta^{17}O$ values typically around -22 to -24 ‰ (e.g., Itoh et al., 2004; Makide et al., 2013; Bodénan et al., 2014; Ushikubo et al., 2017), that is indistinguishable from the O isotope composition of the A-COR-01 diopside rim ($\Delta^{17}O_{Rim}$ = -24.8 ± 0.5 (2SD) ‰). Moreover, the major element composition of the diopside rim surrounding A-COR-01 is indistinguishable to the compositions of diopside rims found around other types of CAIs (e.g., Bodénan et al., 2014).

Thus, it seems likely that this diopside rim formed in the same isotope reservoir in which most CAI minerals formed. The almost uniform O isotope composition of primary minerals in most nominally unaltered CAIs, notably spinel, could indicate that a homogenisation between distinct ^{16}O-rich and ^{16}O-depleted isotopic reservoirs (e.g., gas and dust, respectively Krot et

al., 2010), took place in the CAI forming region between the formation of the core and rim of A-COR-01. No mineral phase in the core of A-COR-01 contains Si, an essential and very abundant element in diopside ($SiO_2 \sim 50$ wt.%), which implies that Si in these rims had to come from a different source. The identical composition of these rims to similar formations around CAIs with very different cores of melilite and spinel (e.g., Bodénan et al., 2014) suggests that they formed by processes independent from core composition unlike other rims that have been suggested to form by reaction of core minerals with the surrounding environment (e.g., Wark and Boynton, 2001). While rare-earth element (REE) data would be required to confirm this, we tentatively suggest that diopside rims may have formed by later condensation from an isotopically distinct nebular gas than that in which A-COR-01 core minerals formed. This different composition could result from of a separate reservoir with higher Si content. However, an evolution of the reservoir in which corundum and hibonite formed prior to diopside cannot be ruled out..

4.4. Evolution of O isotope composition between core and rim formation

Two hypotheses can be explored to explain the difference in composition between core and rim minerals in A-COR-01. Taking hypothesis 1, a process needs to be invoked to explain the evolution between core and rim O isotope compositions.

The slope of the best-fit line through the dataset (slope = 1.06) precludes mass-dependent processes as a possible explanation for the difference in O isotope composition between rim and core minerals, as any such mechanism would result in a slope ~ 0.5, similar to the terrestrial fractionation line.

Several non-mass-dependent processes have been proposed to explain the range of compositions observed in early solar system products such as refractory inclusions and chondrules. The most favoured models proposed to account for O isotope heterogeneity among

early solar system objects rely on the photo-dissociation of CO molecules influenced by isotopologue-controlled self-shielding (Clayton, 2002). Several locations have been suggested for this process to have taken place such as the pre-collapse molecular cloud from which the solar system formed (Yurimoto and Kuramoto, 2004), the inner part of the accretion disk (Clayton, 2002), or the outer surfaces of the protoplanetary disk (Lyons and Young, 2005). If CO self-shielding is responsible for the change of O isotopic composition between the formation of core and rim minerals in A-COR-01, the influx of O resulting from this process into the CAI forming region(s) must have diminished or stopped during the formation of most CAIs. This diminution or pause is required as the majority of least altered CAIs and their rims display a uniform O isotopic composition, implying a period of stability of the O isotope reservoir in which they formed. While this does not exclude this process as a candidate to explain the evolution of O isotope reservoir(s) in the solar system between CAI and chondrule compositions, it seems unlikely that it could explain the evolution of a single reservoir from which the core of A-COR-01 and subsequent rim diopside formed. Another process that could modify the O isotopic composition of the gas would be the thermal processing of primordial solar water and silicates with interstellar dust (Alexander et al., 2017).

If equilibration between ^{16}O-poor dust and ^{16}O-rich gas is considered (see 4.1.), the environment must have changed in terms of temperature and composition for the rim to form (e.g., Simon et al., 2005), and a higher dust/gas ratio in this rim-forming environment could account for the ^{16}O-depletion measured in the rim of A-COR-01 relative to its core.

In the case of hypothesis 2, it has been shown that refractory inclusions could have been distributed throughout the early solar system, after formation close to the Sun, as far as the comet-forming region (e.g., Simon et al., 2008). A-COR-01 could have formed in a region with a low dust/gas ratio, possibly close to the Sun, and transited to a region with higher dust/gas ratio, leading to a ^{16}O-depleted signature of the inclusion rim relative to that of its core.

4.5. Absence of live ^{26}Al in A-COR-01 core minerals

In a $\delta^{26}Mg^*$ vs $^{27}Al/^{24}Mg$ diagram (Fig. 4a), all Mg isotope analyses of A-COR-01 core minerals, corundum and hibonite, plot far below the canonical isochron (($^{26}Al/^{27}Al)_0 = 5 \times 10^{-5}$, MacPherson et al., 1995; $(^{26}Al/^{27}Al)_0 = 5.25 \times 10^{-5}$, Larsen et al., 2011). These results show that there was very little live ^{26}Al incorporated in A-COR-01 during the formation of hibonite or corundum, with an inferred $(^{26}Al/^{27}Al)_0 = (1.67 \pm 0.31) \times 10^{-7}$. Such depletion relative to the canonical $(^{26}Al/^{27}Al)_0$ has been previously reported in some corundum-hibonite bearing CAIs (Simon et al., 2002; Makide et al., 2013).

While many CAIs are reported to have ^{26}Mg excesses that provide evidence that they once contained live ^{26}Al, those CAIs lacking evidence of ^{26}Al are interpreted as evidence for a heterogeneous distribution in time and/or space of ^{26}Al in the early solar system (Sahijpal and Goswami, 1998; Liu et al., 2009; Liu et al., 2012; Kita et al., 2013; Mishra and Chaussidon, 2014; Kööp et al., 2016a).

Large isotopic variations in the early CAI forming region could also be an explanation for the difference in $(^{26}Al/^{27}Al)_0$ between the two groups of CAIs (e.g., Liu et al., 2009; Liu et al., 2012). Boss (2006) showed that a high spatial heterogeneity in $(^{26}Al/^{27}Al)_0$ and oxygen isotopic compositions could be present in the earliest times in the solar system and could have been homogenised rapidly by large-scale mixing on the scale of 10^3 years. In this case, if the more typical CAI O isotope signature of the rim infers typical CAI material with canonical ^{26}Al content, then the difference in composition between core and rim in A-COR-01 could be caused by formation of CAIs in two distinct O isotopic reservoirs . Both could have low $(^{26}Al/^{27}Al)_0$, similar to signatures have been reported in other early inclusions (Krot, 2009; Krot et al., 2019). The other possibility is that CAIs with low $(^{26}Al/^{27}Al)_0$ could have formed before homogenisation while inclusions with canonical $(^{26}Al/^{27}Al)_0$, and the rim of A-COR-01, formed after this event, which is probably easier to achieve.

In the case of temporal heterogeneity, the most likely scenario is that some CAIs formed before the injection of ^{26}Al into the early solar system (e.g., Makide et al., 2013) from a source outside the solar protoplanetary disk. These CAIs would show only very little sign of live ^{26}Al linked to the galactic background. In such a scenario, A-COR-01 would be among the CAIs that formed before the injection of ^{26}Al.

It is also worth noting that A-COR-01's $(^{26}\text{Al}/^{27}\text{Al})_0 = (1.67 \pm 0.31) \times 10^{-7}$ is smaller than the ^{26}Al/^{27}Al implied for the galactic background ($< 8.4 \times 10^{-6}$, Diehl et al., 2006) by almost an order of magnitude. The composition of A-COR-01 may thus be used to better define the value for the ^{26}Al/^{27}Al galactic background.

4.6. Injection of short-lived radionuclides and O isotope composition

While it has been suggested that the O isotopic composition of early solar system products is decoupled from the abundances of SLRs, A-COR-01 shows an extreme ^{16}O-rich isotope composition and might record and preserve events that have not been recorded or preserved in most other CAIs. The lack of ^{26}Mg excess in A-COR-01 suggests that it formed before the injection or homogenisation of live ^{26}Al, and probably other SLRs (e.g., ^{10}Be, or ^{60}Fe Sahijpal and Soni, 2006; Lugaro et al., 2012) in the early solar system. Here, the combination of extreme O and Mg isotopic compositions in A-COR-01 offer a unique opportunity to evaluate models proposed for modifying the O isotope composition of the early solar system along with the injection of SLRs.

Injection of material from a source outside of the solar system could cause a deviation from the lines of slope ~1 and could explain the offset to the right of the reference lines observed in A-COR-01 and some PLAC grains if the average nebular O isotopic composition was initially different from than that determined by McKeegan et al. (2011) from the Genesis solar wind sample.

The injection of material from a supernova, in addition to SLRs, would be expected to modify the O isotope composition of the early solar system. Ellinger et al. (2010) argues that models using a starting composition close to the solar value reported by McKeegan et al. (2011), tend to shift the solar system O isotope composition towards more ^{16}O-rich values rather than towards more ^{16}O-poor, chondritic, values. Thus, while supernovae cannot be ruled out for the injection of SLRs in the early solar system, they are unlikely to explain the evolution of O isotope composition between the formation of the core minerals of A-COR-01 and its rim. Gounelle and Meibom (2007) suggested that Sun could be used as a test for the supernova origin of SLRs. However, the O isotope composition of the Sun inferred from solar winds collected by Genesis ($\Delta^{17}O = -28.4 \pm 1.8$ ‰, McKeegan et al., 2011) and the composition of A-COR-01 core minerals are far removed the highly ^{17}O-rich composition of the Sun required by the models proposed by Gounelle and Meibom (2007).

Ejecta from a Super-AGB could be consistent with the observed abundances of most SLRs in the early solar system (Lugaro et al., 2012) and explain the injection of ^{26}Al in the solar nebula after the formation of A-COR-01. The expected effects would be compatible with the variation of ~ 10 ‰ in $\Delta^{17}O$ between the core and rim in A-COR-01. However, given the O isotope compositions determined for presolar grains (e.g., Hynes and Gyngard, 2009; Lugaro et al., 2003), it seems likely that such an early nucleosynthetic event would be distinguishable from later processes modifying the O isotope composition of the early solar system (e.g., CO self-shielding, mixing of reservoirs).

Wolf-Rayet stars could also be favourable sources for the injection of ^{26}Al and other SLRs in the solar system (Arnould et al., 2006) and have been predicted to shift O isotopic compositions along the CCAM line in certain cases (Sahijpal and Soni, 2006), which would be a promising scenario to explain the compositional evolution in A-COR-01, although better constraints on

the effects on O-isotopes would be needed to narrow down which precise scenario is the most likely.

5. Conclusions

A-COR-01 is an exceptional object in the great family of exceptional objects that are CAIs. Its discovery shows that such ^{16}O-rich objects were probably more widely distributed across solar system bodies and, while minor in abundance, should be considered as an important solar system component.

A-COR-01's mineralogy, especially the presence of corundum, and extremely ^{16}O-rich composition, suggest that it was among the very first CAIs to form in a ^{16}O-rich environment close to the Sun. The lack of live ^{26}Al in this CAI confirms this hypothesis and shows that ^{26}Al and other SLRs were either distributed heterogeneously when this CAI formed, or that SLRs were injected into the early solar system after the formation of A-COR-01.

A-COR-01 records a change of O isotope composition between the formation of its core and rim. This change could be linked to either an evolution in the O isotope composition of the reservoir in which it formed, or the sampling of two distinct reservoirs. In any case, the results presented here show that O isotope composition of the early solar system might not have been homogeneous in the earliest times, before the formation of most CAIs. Alternatively, if it was homogeneous, the isotope composition of the CAI-forming region evolved in the early solar system between the formation of A-COR-01 core and rim. Dating the core and rim of A-COR-01 would allow for a better understanding of the time interval, but techniques available do not currently allow for this.

The preferred scenario is that A-COR-01 sampled a reservoir in the heterogeneous early solar nebula and that this reservoir's signature was later dissolved by mixing in the disk, before the formation of canonical CAIs.

These constraints are however not sufficient to definitely rule out any of the proposed objects hypothesised to introduce SLRs into the early solar system. The study of early-formed CAIs such as corundum-hibonite inclusions and SLRs has recently gained more importance (Makide et al., 2013; Kita et al., 2013), and the rapidly increasing dataset (Kööp et al., 2016b; Kööp et al., 2016a; Needham et al., 2017; Kööp et al., 2018) should help to better constrain early solar system models.

Additional information

The authors declare that they have no competing financial interests.

Author contributions

All authors discussed the results and implications and contributed to the preparation of the manuscript. I.A. F. and N.A. S. conceived the study and led NanoSIMS measurements. J.-D. B. performed sample characterisation and NanoSIMS measurements. S.S. R. led sample characterisation.

Acknowledgements

References

Arnould M., Goriely S. and Meynet G. (2006) The production of short-lived radionuclides by new non-rotating and rotating Wolf-Rayet model stars. *Astron. Astrophys.* **453**, 653–659.

Bar-Matthews M., Hutcheon I. D., MacPherson G. J. and Grossman L. (1982) A corundum-rich inclusion in the Murchison carbonaceous chondrite. *Geochim. Cosmochim. Acta* **46**, 31–41.

Bodénan J.-D., Starkey N. A., Russell S. S., Wright I. P. and Franchi I. A. (2014) An oxygen isotope study of Wark–Lovering rims on type A CAIs in primitive carbonaceous chondrites. *Earth Planet. Sci. Lett.* **401**, 327–336.

Bonal L., Bourot-Denise M., Quirico E., Montagnac G. and Lewin E. (2007) Organic matter and metamorphic history of CO chondrites. *Geochim. Cosmochim. Acta* 71, 1605–1623.

Boss A. P. (2006) Spatial heterogeneity of ^{26}Al $/^{27}$Al and stable oxygen isotopes in the solar nebula. *Meteorit. Planet. Sci.* **41**, 1695–1703.

Boss A. P. and Goswami J. N. (2006) Presolar cloud collapse and the formation and early evolution of the solar nebula. In Meteorites and the Early Solar System II (eds. D. S. Lauretta and H. Y. McSween Jr.). University of Arizona Press, Tucson. pp. 171–186.

Cameron A. G. W. and Truran J. W. (1977) The supernova trigger for formation of the solar system. *Icarus* **30**, 447–461.

Catanzaro E. J., Murphy T. J., Garner E. L. and Shields W. R. (1966) Absolute Isotopic Abundance Ratios and Atomic Weight of Magnesium. *J. Res. Natl. Bur. Stand.* **70**, 453–458.

Chizmadia L. J., Rubin A. E. and Wasson J. T. (2002) Mineralogy and petrology of amoeboid olivine inclusions in CO3 chondrites: Relationship to parent-body aqueous alteration. *Meteorit. Planet. Sci.* **37**, 1781–1796.

Clayton D. D. (1988) Isotopic anomalies: chemical memory of galactic evolution. *Astrophys. J.* **334**, 191–195.

Clayton R. N. (2002) Self-shielding in the solar nebula. *Nature* **415**, 860–861.

Clayton R. N. and Mayeda T. K. (1977) Correlated Oxygen and Magnesium Isotope Anomalies in Allende Inclusions, I: Oxygen. *Geophys. Res. Lett.* **4**, 295–298.

Clayton R. N., Onuma N., Grossman L. and Mayeda T. K. (1977) Distribution of the Pre-Solar Component in Allende and Others Cabonaceous Chondrites. *Earth Planet. Sci. Lett.* **34**, 209–224.

Davis A. M., Richter F. M., Mendybaev R. A., Janney P. E., Wadhwa M. and McKeegan K. D. (2015) Isotopic mass fractionation laws for magnesium and their effects on ^{26}Al–^{26}Mg systematics in solar system materials. *Geochim. Cosmochim. Acta* **158**, 245–261.

Diehl R., Halloin H., Kretschmer K., Lichti G. G., Schönfelder V., Strong A. W., von Kienlin A., Wang W., Jean P., Knödlseder J., Roques J.-P., Weidenspointner G., Schanne S., Hartmann D. H., Winkler C. and Wunderer C. (2006) Radioactive ^{26}Al from massive stars in the Galaxy. *Nature* **439**, 45–7.

Ebel D. S. and Grossman L. (2000) Condensation in dust-enriched systems. *Geochim. Cosmochim. Acta* **64,** 339–366.

Ellinger C. I., Young P. A. and Desch S. J. (2010) Collateral Effects on Solar Nebula Oxygen Isotopes due to Injection of [26]Al by a Nearby Supernova. *Astrophys. J.* **725**, 1495–1506.

Fahey A. J., Goswami J. N., McKeegan K. D. and Zinner E. K. (1987a) 16O Excesses in Murchison and Murray hibonites: A case against a late supernova injection origin of isotopic anomalies in O, Mg, Ca, and Ti. *Astrophys. J.* **323**, L91–L95.

Fahey A. J., Goswami J. N., McKeegan K. D. and Zinner E. K. (1987b) [26]Al, [244]Pu, [50]Ti, REE, and trace element abundances in hibonites grains from CM and CV meteorites. *Geochim. Cosmochim. Acta* **51**, 329–350.

Foster P. N. and Boss A. P. (1997) Injection of Radioactive Nuclides from the Stellar Source that Triggered the Collapse of the Presolar Nebula. *Astrophys. J.* **489**, 346–357.

Gounelle M., Krot A. N., Nagashima K., and Kearsley A. (2009) Extreme 16O-enrichment in refractory inclusions from the Isheyevo meteorite: Implication for oxygen isotope composition of the Sun. Astrophys. J., 698, L18-L22.

Gounelle M. and Meibom A. (2007) The oxygen isotopic composition of the sun as a test of the supernova origin of [26]Al and [41]Ca. *Astrophys. J.* **664**, L123–L125.

Grossman, J.N., Brearley, A.J., 2005. The onset of metamorphism in ordinary and carbonaceous chondrites. *Meteorit. Planet. Sci.* **40**, 87–122.

Hynes K. M. and Gyngard F. (2009) The Presolar Grain Database: http://presolar.wustl.edu/~pgd. *40th Lunar Planet. Sci. Conf.*, (Abstract #**1198**).

Ireland T. R. (1988) Correlated morphological , chemical , and isotopic characteristics of hibonites from the Murchison carbonaceous chondrite. *Geochim. Cosmochim. Acta* **52**, 2827–2839.

Itoh S., Kojima H. and Yurimoto H. (2004) Petrography and oxygen isotopic compositions in refractory inclusions from CO chondrites. *Geochim. Cosmochim. Acta* **68**, 183–194.

Kaur T. and Sahijpal S. (2019) Heterogeneous evolution of the galaxy and the origin of the short-lived nuclides in the early solar system. *Mon. Not. R. Astron. Soc.* **490**, 1620–1637.

Kita N. T., Yin Q.-Z., MacPherson G. J., Ushikubo T., Jacobsen B., Nagashima K., Kurahashi E., Krot A. N. and Jacobsen S. B. (2013) ^{26}Al-^{26}Mg isotope systematics of the first solids in the early solar system. *Meteorit. Planet. Sci.* **48**, 1383–1400.

Kobayashi S., Imai H. and Yurimoto H. (2003) New extreme ^{16}O-rich reservoir in the early solar system. *Geochem. J.* **37**, 663–669.

Kööp L., Davis A. M., Nakashima D., Park C., Krot A. N., Nagashima K., Tenner T. J., Heck P. R. and Kita N. T. (2016a) A link between oxygen, calcium and titanium isotopes in ^{26}Al-depleted hibonite-rich CAIs from Murchison and implications for the heterogeneity of dust reservoirs in the solar nebula. *Geochim. Cosmochim. Acta* **189**, 70–95.

Kööp L., Davis A. M., Nakashima D., Park C., Krot A. N., Nagashima K., Tenner T. J., Heck P. R. and Kita N. T. (2017) Corrigendum to "A link between oxygen, calcium and titanium isotopes in ^{26}Al-poor hibonite-rich CAIs from Murchison and implications for the heterogeneity of dust reservoirs in the solar nebula". *Geochim. Cosmochim. Acta* **212**, 377–379.

Kööp L., Nakashima D., Heck P. R., Kita N. T., Tenner T. J., Krot A. N., Nagashima K., Park C. and Davis A. M. (2018) A mulitelement isotopic study of refractory FUN and F CAIs : Mass-dependent and mass-independent isotope effects. *Geochim. Cosmochim. Acta* **221**, 296–317.

Kööp L., Nakashima D., Heck P. R., Kita N. T., Tenner T. J., Krot A. N., Nagashima K., Park C. and Davis A. M. (2016b) New constraints on the relationship between 26 Al and oxygen

, calcium , and titanium isotopic variation in the early Solar System from a multielement isotopic study of spinel-hibonite inclusions. *Geochim. Cosmochim. Acta* **184**, 151–172.

Krot A. N. (2019) Refractory inclusions in carbonaceous chondrites: Records of early solar system processes (Invited Review). Meteorit. Planet. Sci., 54, 1647-1692.

Krot A. N., Nagashima K., Bizzarro M., Huss G. R., Davis A. M., Meyer B. S. and Ulyanov A. A. (2008) Multiple Generations of Refractory Inclusions in the Metal-Rich Carbonaceous Chondrites Acfer 182/214 and Isheyevo. *Astrophys. J.* **672**, 713–721.

Krot A. N., Nagashima K., Ciesla F. J., Meyer B. S., Hutcheon I. D., Davis A. M., Huss G. R. and Scott E. R. D. (2010) Oxygen Isotopic Composition of the Sun and Mean Oxygen Isotopic Composition of the Protosolar Silicate Dust: Evidence From Refractory Inclusions. *Astrophys. J.* **713**, 1159–1166.

Krot, A.N., Nagashima, K., Simon, S.B., Ma, C., Connolly, H.C., Huss, G.R., Davis, A.M., Bizzarro, M., 2019. Mineralogy, petrography, and oxygen and aluminum-magnesium isotope systematics of grossite-bearing refractory inclusions. Geochemistry 79, 125529. Larsen K. K., Trinquier A., Paton C., Schiller M., Wielandt D., Ivanova M. a., Connelly J. N., Nordlund Å., Krot A. N. and Bizzarro M. (2011) Evidence for Magnesium Isotope Heterogeneity in the Solar Protoplanetary Disk. *Astrophys. J.* **735**, L37.

Liu M.-C., Chaussidon M., Göpel C. and Lee T. (2012) A heterogeneous solar nebula as sampled by CM hibonite grains. *Earth Planet. Sci. Lett.* **327–328**, 75–83.

Liu M.-C., McKeegan K. D., Goswami J. N., Marhas K. K., Sahijpal S., Ireland T. R. and Davis A. M. (2009) Isotopic records in CM hibonites: Implications for timescales of mixing of isotope reservoirs in the solar nebula. *Geochim. Cosmochim. Acta* **73**, 5051–5079.

Lugaro M., Doherty C. L., Karakas A. I., Maddison S. T., Liffman K., García-Hernández D. a., Siess L. and Lattanzio J. C. (2012) Short-lived radioactivity in the early solar system: The Super-AGB star hypothesis. *Meteorit. Planet. Sci.* **47**, 1998–2012.

Lugaro M., Gallino R., Amari S., Zinner E. K. and Nittler L. R. (2003) The effect of heterogeneities in the Interstellar Medium on the CNO isotopic ratios of presolar SiC and corundum grains. *Nucl. Phys. A* **723**, 4–6.

Lyons J. R. and Young E. D. (2005) CO self-shielding as the origin of oxygen isotope anomalies in the early solar nebula. *Nature* **435**, 317–320.

MacPherson G. J., Davis A. M. and Zinner E. K. (1995) The distribution of aluminium-26 in the early Solar System - A reappraisal. *Meteoritics* **30**, 365–368.

Makide K., Nagashima K., Krot A. N. and Huss G. R. (2009) Oxygen Isotopic Compositions of Solar Corundum Grains. *Astrophys. J.* **706**, 142–147.

Makide K., Nagashima K., Krot A. N., Huss G. R., Hutcheon I. D., Hellebrand E. and Petaev M. I. (2013) Heterogeneous distribution of ^{26}Al at the birth of the Solar System: Evidence from corundum-bearing refractory inclusions in carbonaceous chondrites. *Geochim. Cosmochim. Acta* **110**, 190–215.

Marrocchi Y., Euverte R., Villeneuve J., Batanova V., Welsch B., Ferrière L. and Jacquet E. (2019) Formation of CV chondrules by recycling of amoeboid olivine aggregate-like precursors. *Geochim. Cosmochim. Acta* **247**, 121–141.

Marrocchi Y., Villeneuve J., Batanova V., Piani L. and Jacquet E. (2018) Oxygen isotopic diversity of chondrule precursors and the nebular origin of chondrules. *Earth Planet. Sci. Lett.* **496**, 132–141.

McKeegan K. D., Kallio A. P. A., Heber V. S., Jarzebinski G., Mao P. H., Coath C. D., Kunihiro T., Wiens R. C., Nordholt J. E., Moses R. W., Reisenfeld D. B., Jurewicz A. J.

G. and Burnett D. S. (2011) The oxygen isotopic composition of the Sun inferred from captured solar wind. Science **332**, 1528–1532.

Meyer B. S. (2013) Galactic chemical evolution of oxygen in interstellar dust and gas. *Annu. Meteorit. Soc. Meet. 76th,* (abstract #**5255**).

Miller M. F., Franchi I. A., Sexton A. S. and Pillinger C. T. (1999) High precision delta(17)O isotope measurements of oxygen from silicates and other oxides: method and applications. *Rapid Commun. Mass Spectrom.* **13**, 1211–1217.

Mishra R. K. and Chaussidon M. (2014) Timing and extent of Mg and Al isotopic homogenization in the early inner Solar System. *Earth Planet. Sci. Lett.* **390**, 318–326.

Needham A. W., Messenger S., Han J. and Keller L. P. (2017) Corundum-hibonite inclusions and the environments of high temperature processing in the early Solar System. *Geochim. Cosmochim. Acta* **196**, 18–35.

Ouellette N., Desch S. J., Bizzarro M., Boss A. P., Ciesla F. J. and Meyer B. S. (2009) Injection mechanisms of short-lived radionuclides and their homogenization. *Geochim. Cosmochim. Acta* **73**, 4946–4962.

Petaev M. I. and Wood J. A. (2005) Meteoritic Constraints on Temperatures , Pressures , Cooling Rates , Chemical Compositions , and Modes of Condensation in the Solar Nebula. *Chondrites protoplanetary Disk ASP Conf. Ser*. **341**, 373–406.

Petaev M. I. and Wood J. A. (1998) The condensation with partial isolation (CWPI) model of condensation in the solar nebula. *Meteorit. Planet. Sci.* **33**, 1123–1137.

Podosek F. A. (2005) Overview of Origin of Short-lived Radionuclides, Chronology of Refractory Inclusions and Chondrules. *Chondrites protoplanetary Disk ASP Conf. Ser*. **341**, 471–484.

Pouchou J.-L. and Pichoir F. (1987). Basic expression of "PAP" computation for quantitative EMPA, in: Brown, J.D., Packwood, R.H. (Ed.), *11th International Congress on X-ray Optics and Microanalysis*, pp. 249-253.

Russell W. A., Papanastassiou D. A. and Tombrello T. A. (1978) Ca isotope fractionation on the Earth and other solar system materials. *Geochim. Cosmochim. Acta* **42**, 1075–1090.

Sahijpal S. and Goswami J. N. (1998) Refractory phases in primitive meteorites devoid of [26]Al and [41]Ca: Representative samples of first Solar System solids? *Astrophys. J.* **509**, L137–L140.

Sahijpal S. and Soni P. (2006) Stellar nucleosynthetic contribution of extinct short-lived nuclei in the early solar system and the associated isotopic effects. *Meteorit. Planet. Sci.* **41**, 953–976.

Scott E. R. D. and Jones R. H. (1990) Disentangling nebular and asteroidal features of CO3 carbonaceous chondrite meteorites. *Geochim. Cosmochim. Acta* **54**, 2485–2502.

Simon J. I., Young E. D., Russell S. S., Tonui E. K., Dyl K. A. and Manning C. E. (2005) A short timescale for changing oxygen fugacity in the solar nebula revealed by high-resolution [26]Al–[26]Mg dating of CAI rims. *Earth Planet. Sci. Lett.* **238**, 272–283.

Simon S. B., Davis A. M., Grossman L. and McKeegan K. D. (2002) A hibonite-corundum inclusion from Murchison: A first-generation condensate from the solar nebula. *Meteorit. Planet. Sci.* **37**, 533–548.

Simon S. B., Joswiak D. J., Ishii H. A., Bradley J. P., Chi M., Grossman L., Aléon J., Brownlee D. E., Fallon S., Hutcheon I. D., Matrajt G. and McKeegan K. D. (2008) A refractory inclusion returned by Stardust from comet 81P/Wild 2. *Meteorit. Planet. Sci.* **43**, 1861–1877.

Ushikubo T., Kimura M., Kita N. T. and Valley J. W. (2012) Primordial oxygen isotope reservoirs of the solar nebula recorded in chondrules in Acfer 094 carbonaceous chondrite. *Geochim. Cosmochim. Acta* **90**, 242–264.

Ushikubo, T., Tenner, T. J., Hiyagon, H., & Kita, N. T. (2017). A long duration of the 16O-rich reservoir in the solar nebula, as recorded in fine-grained refractory inclusions from the least metamorphosed carbonaceous chondrites. *Geochim. Cosmochim. Acta* **201**, 103–122.

Ushikubo T., Tenner T. J., Hiyagon H. and Kita N. T. (2017) A long duration of the 16O-rich reservoir in the solar nebula, as recorded in fine-grained refractory inclusions from the least metamorphosed carbonaceous chondrites. *Geochim. Cosmochim. Acta* **201**, 103–122.

Wark D. A. and Boynton W. V. (2001) The formation of rims on calcium-aluminum-rich inclusions : Step I-Flash heating. *Meteorit. Planet. Sci.* **36**, 1135–1166.

Wasserburg G. J., Busso M., Gallino R. and Raiteri C. M. (1994) Asymptotic giant branch stars as a source of short-lived radioactive nuclei in the solar nebula. *Astrophys. J.* **424**, 412–428.

Yoneda S. and Grossman L. (1995) Condensation of CaO-MgO-Al2O3-SiO2 liquids from cosmic gases. *Geochim. Cosmochim. Acta* **59**, 3413–3444.

Young E. D. and Russell S. S. (1998) Oxygen Reservoirs in the Early Solar Nebula Inferred from an Allende CAI. *Science* **282**, 452–455.

Yurimoto H. and Kuramoto K. (2004) Molecular cloud origin for the oxygen isotope heterogeneity in the solar system. *Science* **305**, 1763–1766.

Figure captions

Figure 1: Back scattered electron image of A-COR-01. Hibonite laths are visible at the top right corner of the CAI. Cor = corundum; Hib = hibonite; Sp = spinel; Dio = diopside.

Figure 2: Energy dispersive X-ray map of the corundum-hibonite CAI A-COR-01. Mg coloured in red, Ca in green and Al in blue. Corundum (Cor) is typically dark blue, hibonite (Hib) a lighter shade of blue, spinel (Sp) is purple and diopside (Dio) green.

Figure 3: Oxygen three-isotope compositions of the core and rim of A-COR-01. The Terrestrial Fractionation Line (TFL, slope = 0.52), CCAM (slope = 0.94), Y&R (slope = 1.00), PCM (slope = 0.987 ± 0.013 Ushikubo et al., 2012) lines, the solar value inferred by McKeegan *et al.* (2011), and the O isotopic compositions of cores and rims of type A-like CAIs (Bodénan et al., 2014) are given for reference. Error bars are shown as 2σ. Rim minerals are symbolized by circles and core minerals by diamonds

Figure 4: a) $\Delta^{26}Mg^*$ versus $^{27}Al/^{24}Mg$ in corundum, hibonite and diopside in A-COR-01. The red line is the result for a linear regression of the values for corundum and hibonite. The values along the lines correspond to the $(^{26}Al/^{27}Al)_0$ (initial $^{26}Al/^{27}Al$) values associated with these lines. The lines for the canonical value ($4.5\text{-}5 \times 10^{-5}$; MacPherson *et al.*, 1995), supra-canonical value (5.85×10^{-5}; Thrane *et al.*, 2006), and for the galactic background (Diehl et al., 2006) are given for reference. b) is a zoomed-in diagram on hibonite values.

Figure 5: Back scattered electron image of A-COR-01, showing hibonite laths. Note the brighter borders that are interpreted as Ti zoning. Cor = corundum; Hib = hibonite; Sp = spinel.

a)

$\Delta^{26}Mg^*$ (‰)

5.85×10^{-5}

4.5×10^{-5}

8.4×10^{-6}

$(^{26}Al/^{27}Al)_0 = (1.67 \pm 0.31) \times 10^{-7}$

Hibonite
Corundum
Regression line

$^{27}Al/^{24}Mg$

b)

$\Delta^{26}Mg^*$ (‰)

5.85×10^{-5}

4.5×10^{-5}

8.4×10^{-6}

$\delta^{26}Mg^* = 1.51 \pm 3.88 \ (2\sigma) \ ‰$

$^{27}Al/^{24}Mg$
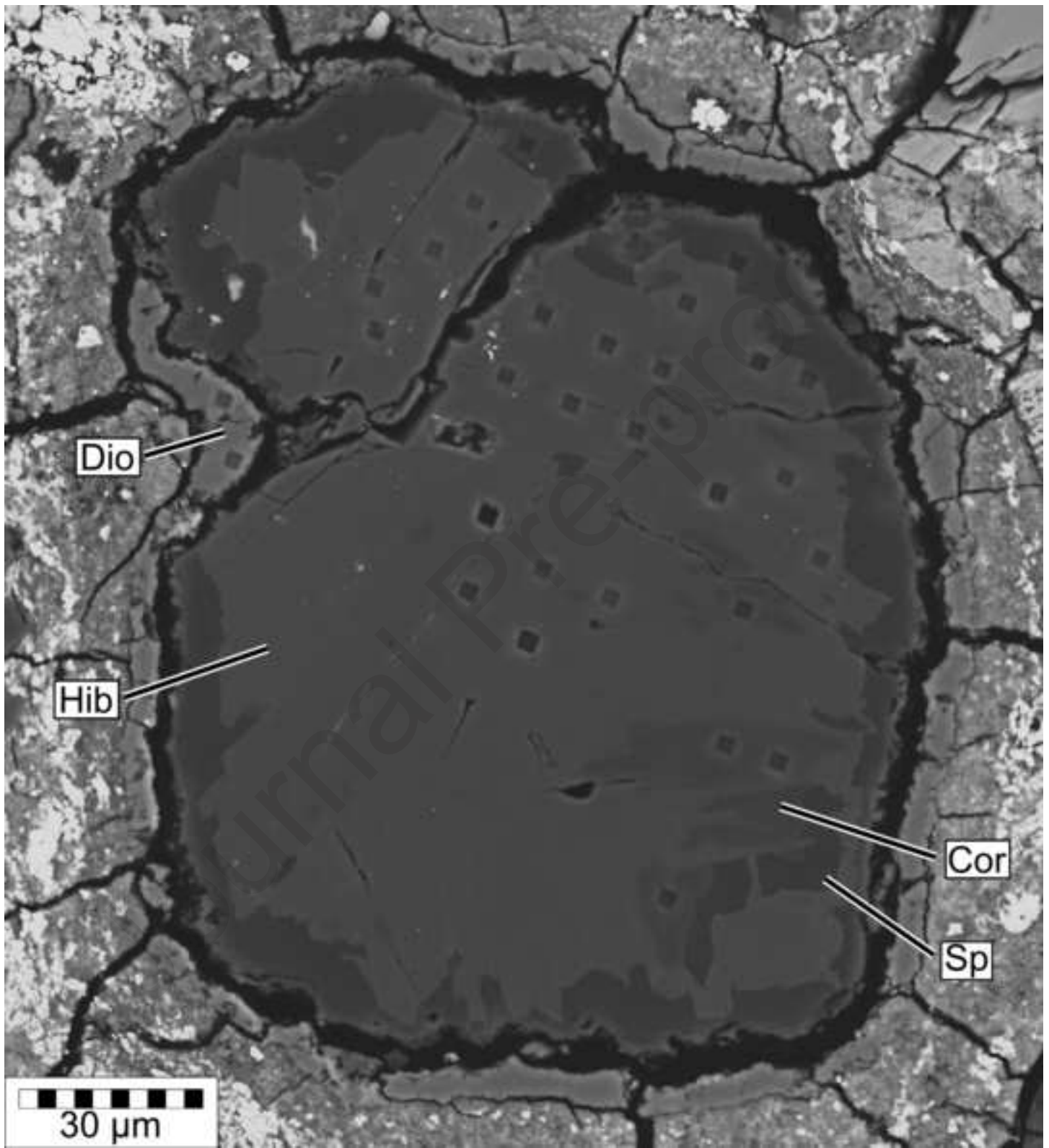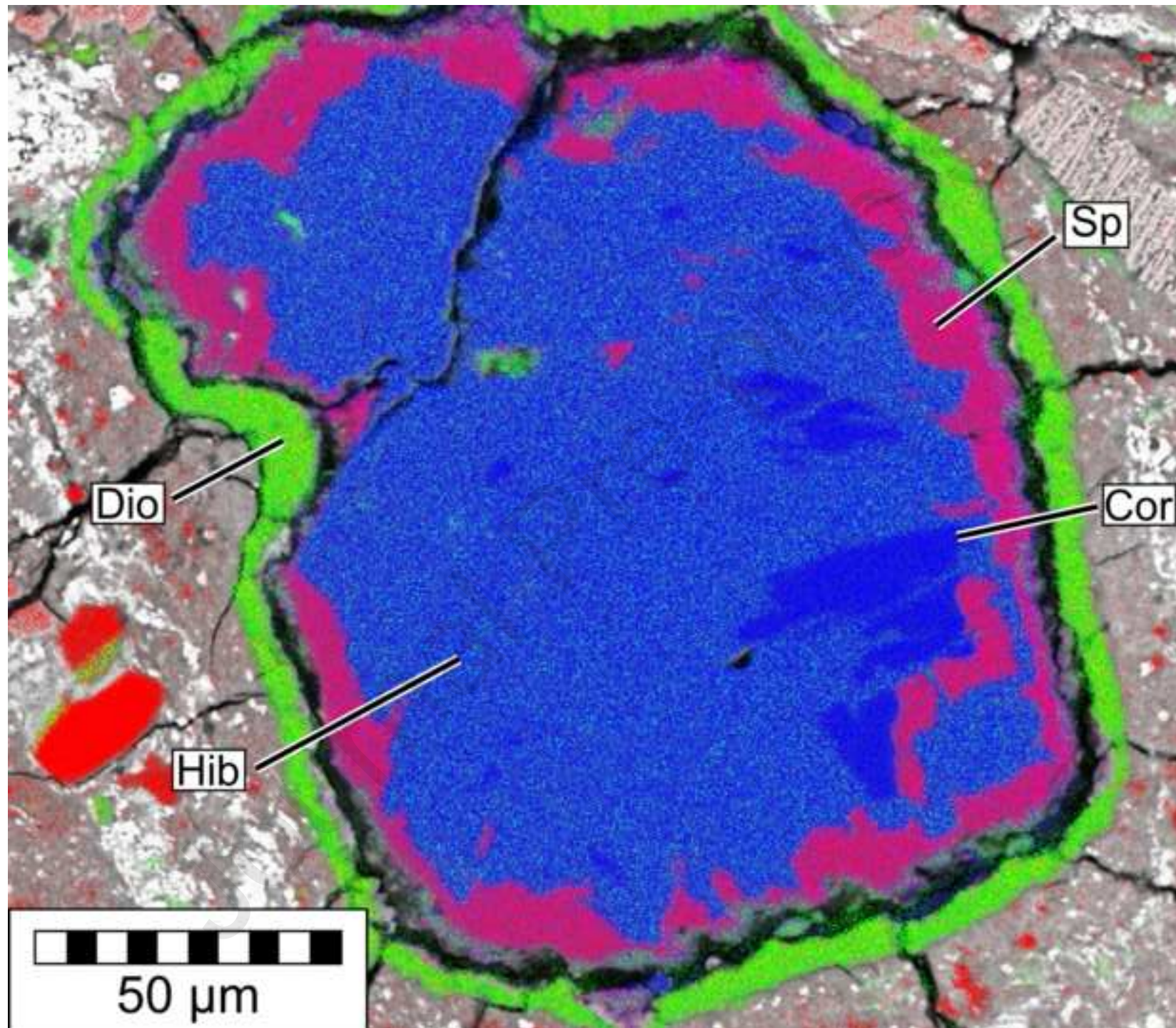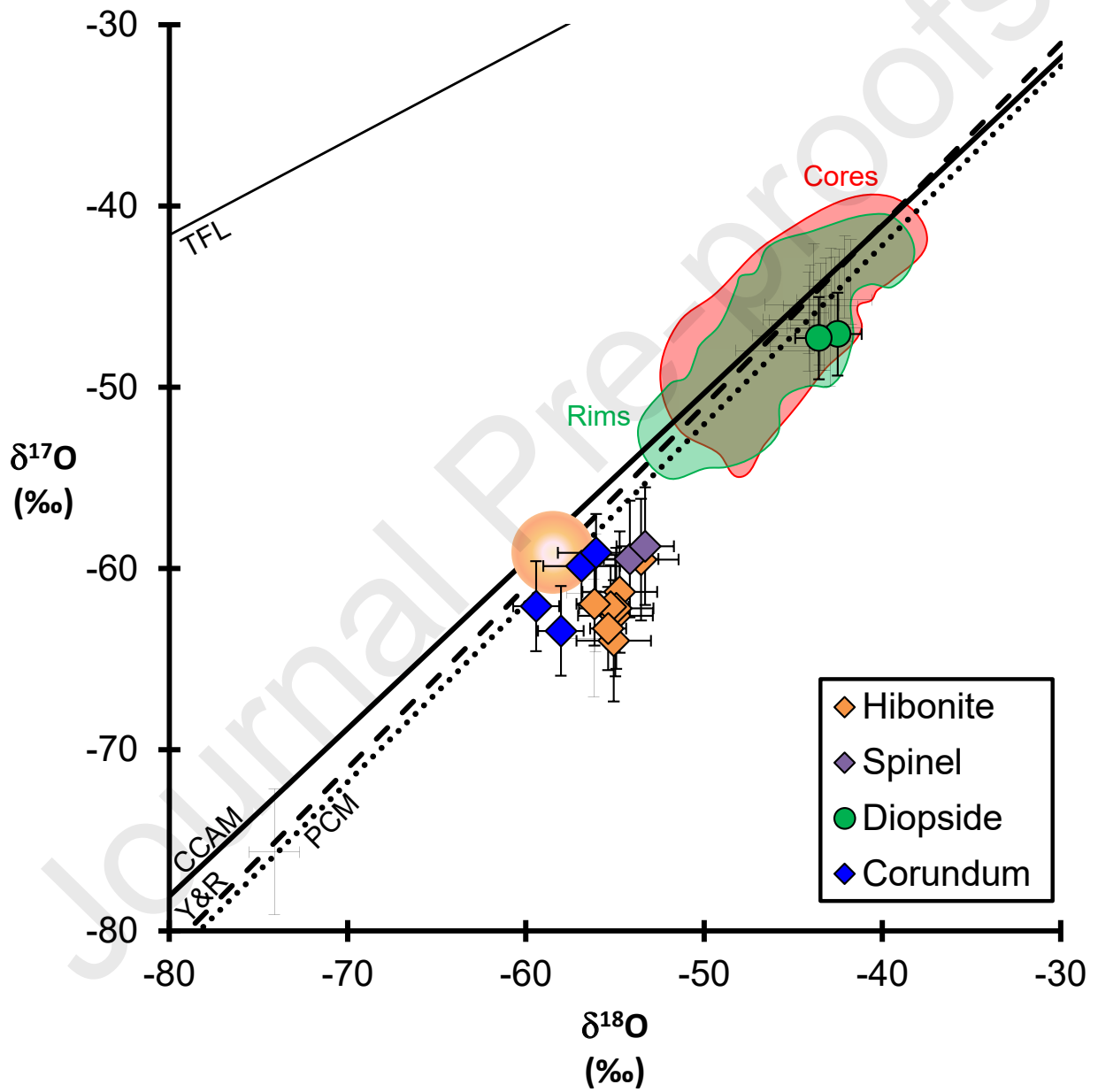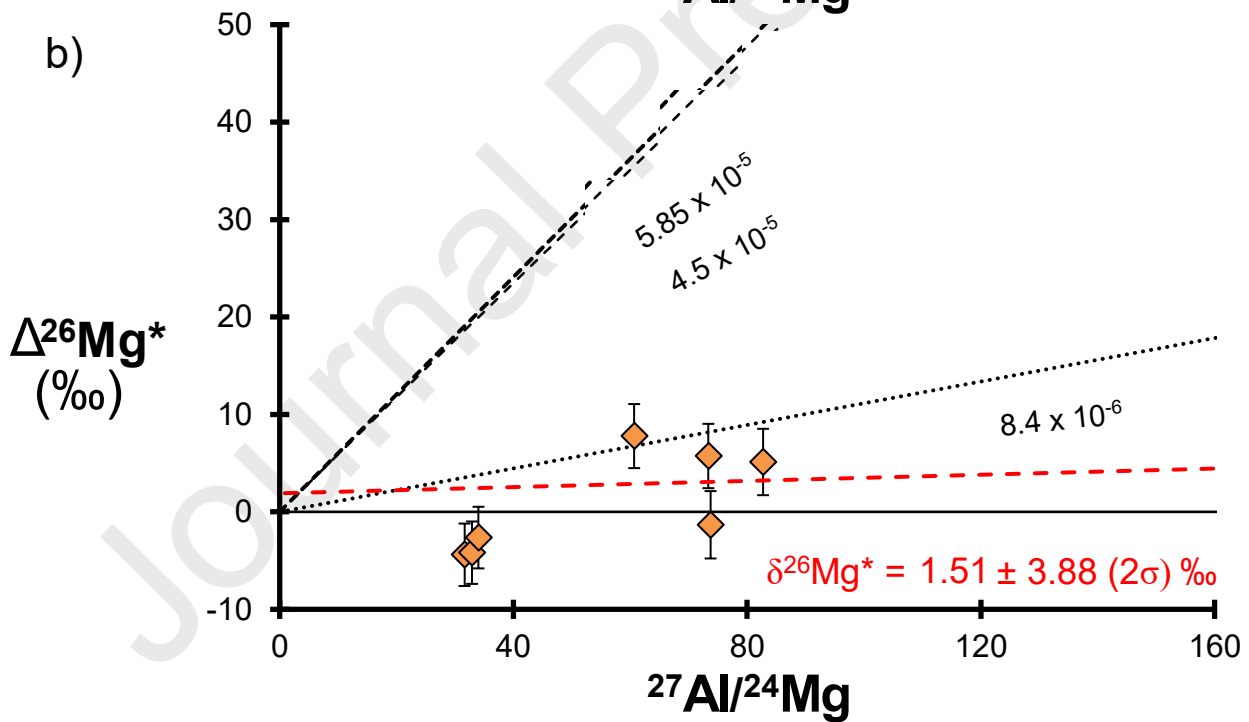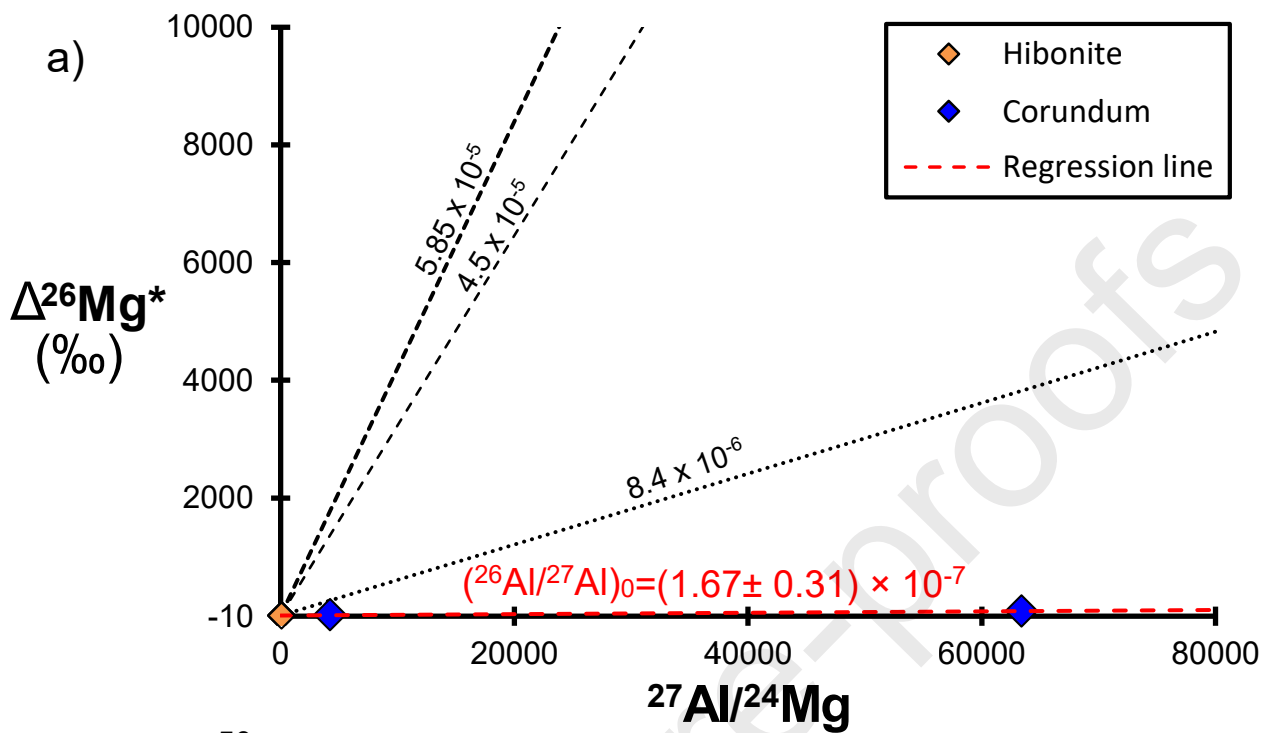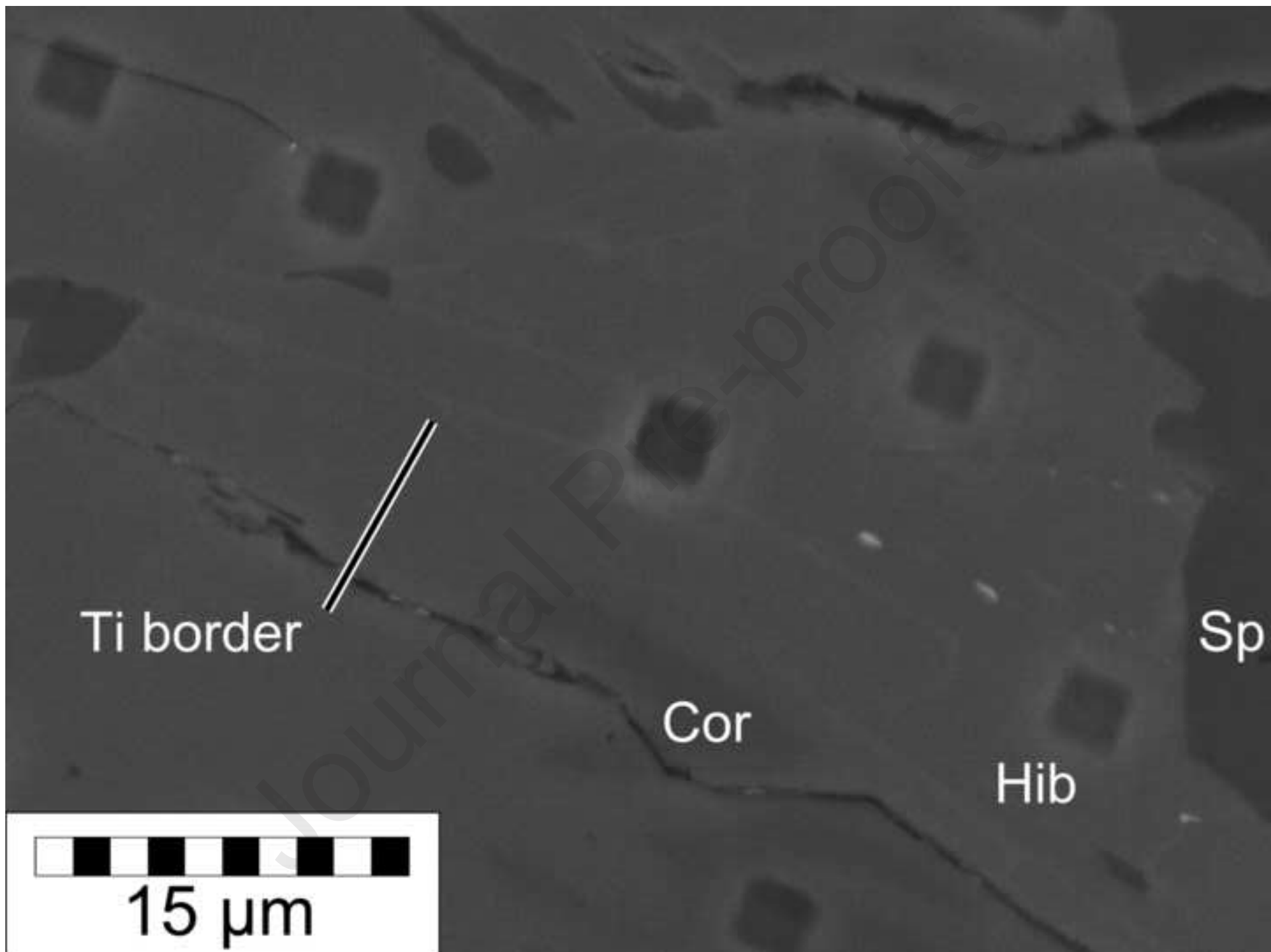
Table captions

Table 1: Major element compositions of mineral phases in A77307-COR-01. Results are given in wt% of oxides.

Table 2: In-situ measurements of oxygen isotope compositions in A77307-COR-01. The data are presented as $\delta^{18}O$, $\delta^{17}O$, $\Delta^{17}O$ in permil (‰) and their associated errors at 2SD.

Table 3: In-situ measurements of magnesium-isotope compositions in A77307-COR-01. The data are presented as $\delta^{25}Mg$, $\delta^{26}Mg$, in permil (‰), $^{27}Al/^{24}Mg$, and their associated errors at 2SD.

Table 1: Major element compositions of mineral phases in A77307-COR-01. Results are

given in wt% of oxides.

	Rim							Core																
	Diopside			Spinel		Corundum		Hibonite																
	#1	#2	#3	#1	#2	#1	#2	#1	#2	#3	#4	#5	#6	#7	#8	#9	#10	#11	#12	#13	#14	#15	#16	#17
SiO_2	52.47	53.70	51.25	0.55	0.19	0.06	0.07	0.07	0.06	0.06	0.14	0.07	0.06	0.06	0.07	0.07	0.07	0.11	0.08	0.06	0.13	0.43	0.06	0.07
TiO_2	1.42	1.44	2.22	0.62	0.67	0.13	0.23	1.48	1.70	1.93	5.33	1.82	1.37	1.55	0.70	1.37	2.36	4.14	2.15	2.40	2.02	2.13	0.91	0.91
Al_2O_3	21.99	2.21	23.73	69.29	70.48	99.33	99.02	87.74	87.30	87.22	83.80	87.68	87.82	88.66	89.75	88.57	88.40	84.91	87.98	87.70	87.88	87.04	88.54	91.71
FeO	0.66	0.46	1.61	0.28	0.25	0.12	0.11	0.14	0.09	0.14	0.10	0.11	0.11	0.12	0.12	0.14	0.17	0.19	0.13	0.17	0.13	0.14	0.09	0.05
MnO	0.02	0.01	0.02	0.01	0.01	0.00	0.00	0.00	0.00	0.00	0.00	0.00	0.00	0.02	0.00	0.00	0.00	0.01	0.01	0.00	0.00	0.00	0.00	0.00
MgO	17.71	18.07	16.06	28.26	28.89	0.02	0.10	0.70	0.86	1.04	3.46	0.94	0.71	0.83	0.34	0.80	1.08	3.96	1.01	1.20	1.02	1.29	0.58	0.49
CaO	24.75	24.75	23.58	0.13	0.12	0.54	0.21	8.37	8.30	8.44	8.08	8.45	8.42	8.10	8.31	8.35	8.28	7.83	8.41	8.34	8.33	8.20	8.42	8.32
Na_2O	0.01	0.00	0.06	0.01	0.02	0.00	0.00	0.00	0.00	0.00	0.00	0.00	0.00	0.00	0.00	0.00	0.00	0.00	0.01	0.00	0.02	0.01	0.00	0.00
K_2O	0.00	0.00	0.02	0.00	0.00	0.00	0.00	0.00	0.00	0.00	0.00	0.00	0.00	0.00	0.00	0.00	0.00	0.00	0.00	0.00	0.01	0.01	0.00	0.00
Rb_2O	n.d.	n.d.	n.d.	0.02	0.02	n.d.	n.d.	n.d.	n.d.	n.d.	n.d.	n.d.	n.d.	n.d.	n.d.	n.d.	n.d.	n.d.	n.d.	n.d.	n.d.	n.d.	n.d.	n.d.
ZnO	n.d.	n.d.	n.d.	n.d.	n.d.	n.d.	n.d.	0.00	0.00	0.00	0.03	0.00	0.00	0.01	0.02	0.00	0.00	0.02	0.00	0.03	0.01	0.00	0.00	0.00
Cl	0.01	0.00	0.01	0.01	0.01	0.00	0.00	0.01	0.00	0.00	0.00	0.01	0.00	0.00	0.01	0.01	0.00	0.00	0.01	0.00	0.01	0.01	0.01	0.01
Cr_2O_3	0.03	0.04	0.15	0.27	0.28	0.00	0.00	0.03	0.00	0.01	0.03	0.02	0.00	0.01	0.00	0.02	0.02	0.05	0.00	0.01	0.01	0.02	0.00	0.00
SO_2	0.08	0.04	0.08	n.d.	n.d.	0.02	0.01	0.02	0.02	0.02	0.01	0.01	0.01	0.02	0.02	0.02	0.01	0.01	0.01	0.02	0.01	0.02	0.01	0.02
P_2O_5	0.00	0.00	0.07	0.00	0.01	0.00	0.01	n.d.	n.d.	n.d.	n.d.	n.d.	n.d.	n.d.	n.d.	n.d.	n.d.	n.d.	n.d.	n.d.	n.d.	n.d.	n.d.	n.d.
Total	99.16	100.73	98.86	99.43	100.96	100.21	99.76	98.56	98.34	98.85	100.99	99.11	98.56	99.32	99.35	99.33	100.46	101.21	99.74	100.00	99.49	99.34	98.62	101.58
Oxygens	6	6	6	32	32	3	3	19	19	19	19	19	19	19	19	19	19	19	19	19	19	19	19	19

Si	1.918	1.925	1.883	0.106	0.037	0.001	0.001	0.007	0.007	0.007	0.016	0.008	0.007	0.006	0.008	0.008	0.007	0.012	0.009	0.006	0.015	0.048	0.007	0.008
Al	0.086	0.093	0.161	15.613	15.654	1.989	1.989	11.719	11.686	11.631	11.012	11.654	11.734	11.732	11.865	11.730	11.604	11.115	11.617	11.576	11.625	11.546	11.802	11.846
Ti	0.039	0.039	0.061	0.089	0.094	0.002	0.003	0.126	0.146	0.164	0.447	0.154	0.117	0.131	0.059	0.116	0.197	0.346	0.181	0.202	0.171	0.180	0.077	0.075
Fe	0.020	0.014	0.050	0.044	0.039	0.002	0.002	0.013	0.008	0.013	0.009	0.010	0.011	0.011	0.011	0.013	0.016	0.017	0.013	0.016	0.012	0.013	0.008	0.004
Mn	0.001	0.000	0.001	0.001	0.002	0.000	0.000	0.000	0.000	0.000	0.000	0.000	0.000	0.002	0.000	0.000	0.000	0.001	0.001	0.000	0.000	0.000	0.000	0.000
Mg	0.965	0.966	0.879	8.053	8.117	0.000	0.002	0.118	0.146	0.175	0.576	0.159	0.120	0.140	0.053	0.133	0.178	0.655	0.168	0.200	0.170	0.216	0.098	0.081
Zn	n.d.	n.d.	n.d.	n.d.	n.d.	n.d.	n.d.	0.000	0.000	0.000	0.003	0.000	0.000	0.001	0.001	0.000	0.000	0.002	0.000	0.002	0.001	0.000	0.000	0.000
Ca	0.969	0.951	0.928	0.026	0.024	0.010	0.004	1.017	1.010	1.023	0.966	1.021	1.022	0.974	0.999	1.005	0.987	0.932	1.011	1.000	1.003	0.989	1.021	0.977
Na	0.000	0.000	0.004	0.003	0.006	0.000	0.000	0.000	0.000	0.001	0.000	0.000	0.000	0.000	0.001	0.001	0.000	0.002	0.000	0.005	0.002	0.001	0.000	
K	0.000	0.000	0.001	0.000	0.000	0.000	0.000	0.001	0.000	0.000	0.000	0.000	0.000	0.001	0.000	0.000	0.001	0.000	0.000	0.000	0.001	0.001	0.000	0.000
Rb	n.d.	n.d.	n.d.	0.003	0.003	n.d.	n.d.	n.d.	n.d.	n.d.	n.d.	n.d.	n.d.	n.d.	n.d.	n.d.	n.d.	n.d.	n.d.	n.d.	n.d.	n.d.	n.d.	n.d.
Cl	0.001	0.000	0.001	0.003	0.004	0.000	0.000	0.002	0.000	0.000	0.000	0.002	0.000	0.000	0.001	0.002	0.000	0.000	0.002	0.000	0.001	0.002	0.002	0.002
Cr	0.001	0.001	0.001	0.040	0.042	0.000	0.000	0.002	0.000	0.000	0.002	0.001	0.000	0.001	0.000	0.002	0.002	0.004	0.000	0.001	0.001	0.002	0.000	0.000
P	0.000	0.000	0.002	0.000	0.001	n.d.	n.d.	n.d.	n.d.	n.d.	n.d.	n.d.	n.d.	n.d.	n.d.	n.d.	n.d.	n.d.	n.d.	n.d.	n.d.	n.d.	n.d.	n.d.
Total	4.000	3.989	3.973	23.981	24.023	2.003	2.001	13.006	13.004	13.014	13.031	13.010	13.010	12.997	13.001	13.011	12.993	13.083	13.003	13.003	13.005	12.999	13.016	12.993

Table 2: In-situ measurements of oxygen isotope compositions in A77307-COR-01.

The data are presented as $\delta^{18}O$, $\delta^{17}O$, $\Delta^{17}O$ in permil (‰) and their associated errors at 2SD.

	$\delta^{17}O$ (‰)	2SD $\delta^{17}O$	$\delta^{18}O$ (‰)	2SD $\delta^{18}O$	$\Delta^{17}O$ (‰)	2SD $\Delta^{17}O$
Corundum (Core)						
A77307-COR-01_Cor_01	-59.9	2.1	-56.9	2.1	-30.3	2.6
A77307-COR-01_Cor_02	-59.1	2.1	-56.1	2.1	-30.0	2.6
A77307-COR-01_Cor_03	-62.1	2.5	-59.4	1.3	-31.2	2.7
A77307-COR-01_Cor_04	-63.4	2.5	-58.0	1.3	-33.3	2.6
Mean	**-61.1**		**-57.6**		**-31.2**	
2 Std Deviations	**4.0**		**2.9**		**3.0**	
Hibonite (Core)						
A77307-COR-01_Hib_01	-62.6	3.3	-55.0	2.1	-34.0	3.7
A77307-COR-01_Hib_02	-64.0	3.4	-55.1	2.1	-35.4	3.7
A77307-COR-01_Hib_03	-61.3	3.3	-54.7	2.1	-32.8	3.7
A77307-COR-01_Hib_04	-62.2	3.3	-54.9	2.1	-33.6	3.7
A77307-COR-01_Hib_05	-59.5	3.4	-53.5	2.1	-31.7	3.7
A77307-COR-01_Hib_06	-62.1	2.3	-55.2	1.0	-33.4	2.4
A77307-COR-01_Hib_07	-62.0	2.3	-56.2	1.0	-32.8	2.4
A77307-COR-01_Hib_08	-63.3	2.3	-55.4	1.0	-34.5	2.4
Mean	**-62.1**		**-55.0**		**-33.5**	
2 Std Deviations	**2.7**		**1.5**		**2.3**	
Spinel (Core)						
A77307-COR-01_Sp_01	-59.5	3.2	-54.2	1.6	-31.3	3.4
A77307-COR-01_Sp_02	-58.8	3.2	-53.3	1.6	-31.1	3.4
Mean	**-59.1**		**-53.7**		**-31.2**	
2 Std Deviations	**1.0**		**1.2**		**0.4**	

Diopside (Rim)

A77307-COR-01_Dio_01	-47.1	2.3	-42.5	1.3	-25.0	2.5
A77307-COR-01_Dio_02	-47.3	2.3	-43.6	1.3	-24.6	2.5
Mean	**-47.2**		**-43.0**		**-24.8**	
2 Std Deviations	**0.3**		**1.5**		**0.5**	

Table 3: In-situ measurements of magnesium isotope compositions in A77307-COR-01.

The data are presented as δ^{25}Mg, δ^{26}Mg in permil (‰), ^{27}Al/^{24}Mg, and their associated errors at 2SD.

	δ^{25}Mg (‰)	2SD δ^{25}Mg	δ^{26}Mg (‰)	2SD δ^{26}Mg	^{27}Al/^{24}Mg	2SD ^{27}Al/^{24}Mg	δ^{26}Mg* (‰)	2SD δ^{26}Mg*
Corundum (Core)								
#1	-41.3	34.7	-3.7	32.6	63376.71	0.88	75.5	47.6
#2	-18.3	10.2	-22.0	9.7	4200.31	0.39	13.5	14.0
Hibonite (Core)								
#1	-17.3	1.9	-25.7	2.7	60.67	0.03	7.8	3.3
#2	-14.7	1.9	-22.9	2.7	73.37	0.03	5.7	3.3
#3	-14.4	2.0	-22.9	2.7	82.73	0.05	5.1	3.4
#4	-16.8	2.3	-36.9	2.2	31.63	0.04	-4.4	3.2
#5	-16.8	2.3	-36.7	2.2	32.92	0.04	-4.2	3.2
#6	-17.1	2.2	-35.8	2.2	34.02	0.06	-2.6	3.2
#7	-17.2	2.6	-34.8	2.2	73.74	0.05	-1.3	3.5
Diopside (Rim)								
#1	11.1	3.7	3.4	1.9	0.25	0.03	-18.4	4.1

Declaration of interests

☒ The authors declare that they have no known competing financial interests or personal relationships that could have appeared to influence the work reported in this paper.

☐The authors declare the following financial interests/personal relationships which may be considered as potential competing interests: